HIGH SPATIAL RESOLUTION CLOUD CHARACTERISATION FOR TOVS AND ATOVS DATA ANALYSIS

Michael J. Uddstrom, Warren R. Gray and John W. Kidson
National Institute of Water and Atmospheric Research
PO Box 14 901, Wellington
New Zealand

1. INTRODUCTION

ISCCP data products suggest the total cloud amount over the mid-latitudes and tropics (Rossow and Schiffer, 1991) lies in the range 70 - 80%, while the global mean is about 62%. Using a CO_2 slicing method, Menzel et al. (1993) find that the global average for all clouds, both semi-transparent and opaque, is about 75%. However, the number of cloudy and partly cloudy fields of view (fovs) detected by the TOVS operational cloud detection algorithms is rather lower than these estimates might suggest, indicating cloud contamination of HIRS data remains a problem. With the launch of AMSU, direct measurements of emission from cloud liquid water droplets (over oceans) and scattering by ice particles (over land, and oceans) will enable precipitation rates to be inferred (Grody et al. 1996) in many situations. However, to make full use of AMSU and HIRS data, cloud, cloud-liquid phase and precipitation contaminants within the ifovs of these instruments need to be identified. One approach to an improved understanding of these problems is to use collocated data from the AVHRR to help identify these "contaminants". In the research reported here we will present results which indicate what can be achieved with AVHRR Bayesian classification algorithms utilising cloud field radiometric and spatial features to estimate cloud cover, cloud-type and rain-rate. The algorithms used are based on work reported by Uddstrom et al., (1997) for cloud discrimination, and Uddstrom and Gray (1996) for cloud classification and rain-rate prediction.

2. METHODOLOGY AND THEORETICAL BASIS

The problem of detecting the presence of cloud, or of some type of cloud in a fov can be thought of as a classification problem. Thus given the *a priori* knowledge that some observable belongs to one of m possible classes (ω_i, i = 1, m), a vector of measurements (**f**, the feature vector) that in some sense characterise the observable, and the assumption that all misclassifications are equally costly, then the posterior probability $P(\omega_i|\mathbf{f})$, is the conditional probability that the observable belongs to class ω_i. Accordingly, the best classification of the observable is the one that maximises this probability, i.e. it belongs to class i if

$$P(\omega_i|\mathbf{f}) > P(\omega_j|\mathbf{f}), \quad \forall j \neq i \tag{1}$$

From Bayes theorem;

$$P(\omega_i \mid \mathbf{f}) = P(\mathbf{f} \mid \omega_i)P(\omega_i) \; / \; \sum_{j=1}^{m} P(\mathbf{f} \mid \omega_j)P(\omega_j) \qquad (2)$$

where $P(\omega_i)$ is the *a priori* probability that the observable belongs to class i. If the underlying distribution is multivariate Gaussian, and the measurement errors are unbiased; a measure of the distance of feature $\mathbf{f}$ from class i can specified by the discriminant function in equ (3):-

$$g_i(\mathbf{f}) = log[P(\omega_i) \; / \; (2\Pi^{\frac{m}{2}} \mid \mathbf{S}_{fi} \mid^{\frac{1}{2}})] - \tfrac{1}{2}(\mathbf{f} - \bar{\mathbf{f}}_i)^T \mathbf{S}_{f_i}^{-1} (\mathbf{f} - \bar{\mathbf{f}}_i) \qquad (3)$$

where $\bar{\mathbf{f}}_i$ and S_{fi} are the mean (vector) and covariance (matrix) for class i and some set of features.

The feature vector elements may include simple spectral measurements and/or complex spatial measures such as spatial texture (Parikh, 1977). However, the accuracy, or skill of the resulting discriminant function will be dependent upon the separability of the m classes in feature space as specified by the class mean and covariance statistics and the apriori probabilities of the classes. Measurement noise will also limit the separability of the classes. Of course, $\bar{\mathbf{f}}_i$ and S_{fi} must be determined from "labelled" samples of the m specified classes.

In the case of the cloud-mask problem there are just two possible states for each instantaneous field-of-view (ifov) - clear or cloudy - although the posterior probability for either class may not be close to unity, implying that the measurements perhaps represent a partly cloudy observation. For the cloud-type classification problem, there will be as many classes as there are cloud types identified in the labelled samples.

Here sample labelling is performed by an analyst who identifies (or labels) specific cloud classes in a training sample dataset. A key premise of this approach is that meteorologically significant cloud classes are identified. Although these classes are not necessarily separable in the available feature space, neither are they determined by a clustering algorithm which while producing "cloud classes" having maximal separation in the chosen feature space, are perhaps difficult to identify meteorologically, and change with feature selection. The approach followed here is fully outlined in Uddstrom and Gray (1996).

3. DATA

Since the skill of Bayesian classification methods is critically dependent upon the span of the labelled data sets used to develop the discriminant model equations, two different data sets have been developed. For the cloud classification and rain-rate estimation problem, Local Area Coverage (LAC) resolution AVHRR data have been collocated at full radiometric resolution with three S-Band weather radars[1] situated at Mt. Tamahunga (36.30°S, 174.71°E, 453 m above mean sea level (amsl)), Outlook Hill (41.31°S, 174.64°E, 534 m amsl) and Rakaia (43.79°S, 172.02°E, 124 m amsl) (see Fig.1). Necessarily, the geo-

[1] Owned and operated by the Meteorological Service of New Zealand Ltd.

graphical constraints imposed by the need to collocate the satellite data with radar observations probably limits the application of the resulting algorithms to the temperate mid-latitudes. However, the data set does extend from 1994 to the present thus enabling many different meteorological situations to be captured. For the cloud detection problem, no radar collocation data are required, so the geographical coverage can be extended beyond that used by the cloud classification and rain-rate algorithms. To this end, similar high resolution AVHRR data were archived for 9 months (from July 1996 to April 1997) over three disparate oceanic regions (see Fig). These regions include tropical and sub-Antarctic waters, as well as a region having high spatial gradients in Sea Surface Temperature (SST). Data from an additional region, called SALPEX_3 which includes both land and ocean (Fig. 1) were also available (from 1994 to the present).

3.1 Satellite Data

The AVHRR instruments used here (NOAA11, NOAA12 and NOAA14) are five channel devices, having nominal spectral intervals:- 0.55 - 0.68 μm (R_1); 0.725 - 1.1 μm (R_2); 3.55 - 3.93 μm (T_3); 10.5 - 11.5 μm (T_4), and 11.5 - 12.5 μm (T_5). The data are at LAC spatial resolution, yielding an instantaneous field of view (ifov) of 1.1 km at nadir, and are stored and analysed at full 10 bit radiometric resolution.

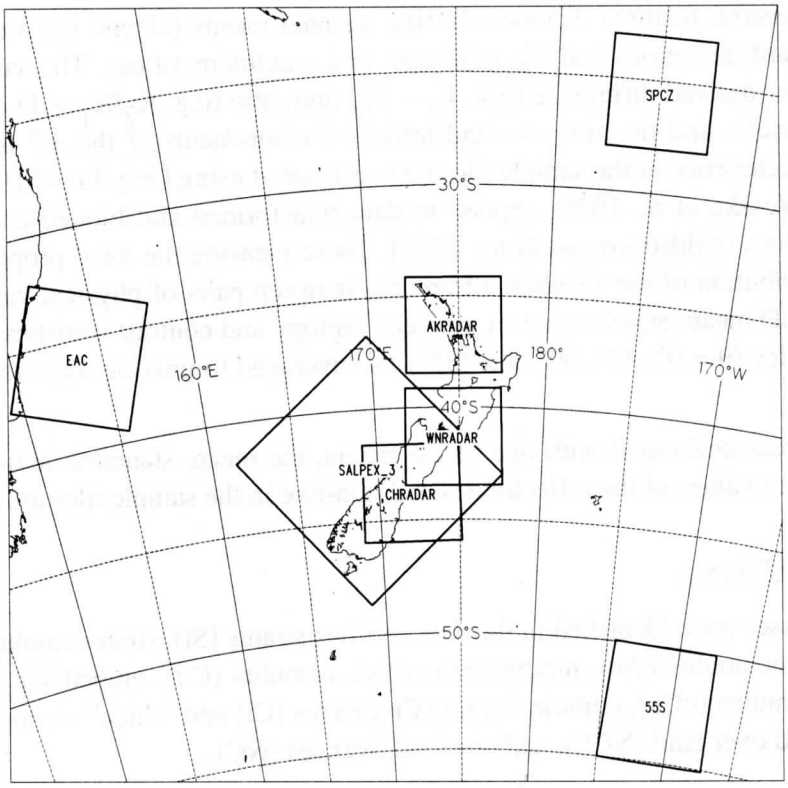

Figure 1: Areas from which AVHRR data were archived in order to develop the Bayesian cloud-mask (SPCZ, 55S, EAC, SALPEX_3, AKRADAR, WNRADAR and CHRADAR), cloud-type and rain rate (AKRADAR, WNRADAR and CHRADAR) algorithms.

Channel 1 and 2 bi-directional reflectances of the scene were calculated using the pre-launch calibration coefficients and a correction for the solar view angle. The longwave ther-

mal channels were calibrated using the non-linear method given in Planet (1989). Regions of sunglint, or specular reflection, were identified through examination of the sun – ifov – sensor geometry using the method of Stowe et al. (1991). Finally, the AVHRR data are remapped onto Lambert Conformal projections at 1 km resolution.

3.2 Radar Data

All three radars operate at a wavelength of 5.6 cm, have nominal beam widths of 0.86°, 2 km range bins and are controlled by Ericsson Weather Information System (EWIS) software. They generate polar-volume scans at 10 elevations, the lowest four of which are 0.5°, 0.9°, 1.3° and 2.5°. Full volume scans are carried out every 15 minutes and take 2 minutes to acquire. Post processing of these data allow corrections to be estimated for errors induced by hill and sea clutter, attenuation, beam blocking and vertical profile of reflectivity effects. Rain-rates were calculated using the standard Z-R relationship for frontal rain ($Z\ (mm^6\ m^{-3}) = 200\ R^{1.6}$), and rectified onto the same grid as that used for the satellite data (see Uddstrom and Gray, 1996).

3.3 Features

Radiometric and spatial characteristics were computed for all labelled 8×8 ifov sample tiles. Radiometric features include AVHRR channel means (albedo and radiance temperature), standard deviations and tile minimum and maximum values. The same statistics are computed for derived difference (e.g. $T_4 - T_5$) and ratio (e.g. $R_2/R_1 - 1$) channels, the infrared radiances, and the emissive and reflective components of the 3.7 μm channel. The spatial characteristics of the sample tiles were estimated using Grey Level Difference (GLD) statistics (Weszka et al. 1976) applied to data transformed and binned according to their physical values (Uddstrom and Gray, 1996). These measure the local properties of the frequency distribution of the absolute differences between pairs of physical values in the sample tiles. GLD mean, angular second moment, entropy and contrast statistics were computed for four angles ($\theta = 0°, 45°, 90°$ and 135°) and averaged to provide directionally independent values.

For those areas collocated with one of the radars, the mean, standard deviation, minimum and maximum values of the reflectivities and rain-rate in the sample tiles are computed.

3.4 Labelled Classes

Thirteen classes were identified in the data archive; stratus (St), stratocumulus (Sc), altostratus (As), altocumulus (Ac), nimbostratus (Ns), cumulus (Cu), embedded cumulus (eCu), open-cell cumulus (oCu), cumulonimbus (Cb), cirrus (Ci) and "thick" cirrus (CiC), together with no cloud over land (NCL), and no cloud over sea (NC).

4. CLOUD-TYPE CLASSIFICATION

From the labelled training samples Bayesian discriminant function classifiers were tested for different selections of feature vector elements. In each case, because of limited samples of eCu and oCu data, the classification was performed on just 11 (of the potential 13) classes.

Data from these samples were combined with those in the Cu class - extending the span of that class to include mesoscale convective clusters. Also, due to the differing radiometric data available, separate equations are defined for day and night data. Table 1 shows the cloud-type classification skill of 9 different discriminant models derived from differing feature vectors. Here, the column labelled "Fraction Correct" is just the sum of the diagonal elements of the resulting contingency table over the total sample size, while that labelled Kuipers Performance Index (Murphy and Katz, 1985) measures the skill of each discriminant function.

Table 1: Discriminant function skill for an 11 class classifier (NC, NCL, St, Sc, As, Ac, Ns, Cu, Cb, Ci, CiC) and sample sizes 1340 for day data, models 1 to 4, and 3657 for night data, models 5 to 9. In all cases the prior probability was 0.091 (i.e. 1/11) and all samples are classified.

Model No.	Features (where:- $\nu_2 = (R_2/R_1 - 1)$, μ =GLD mean, asm = GLD angular second moment and ent = GLD entropy)	Fraction Correct	Kuipers Performance Index
1	ν_2	0.26	0.22
2	ν_2, T_4	0.47	0.44
3	ν_2, T_4, ent (T_4)	0.59	0.55
4	ν_2, T_4, ent (T_4), R_2, ent (R_2), ($T_4 - T_5$), ent ($T_4 - T_5$)	0.74	0.72
5	T_4	0.44	0.37
6	T_4, ($T_4 - T_3$)	0.46	0.41
7	T_4,($T_4 - T_3$), ($T_4 - T_5$)	0.51	0.46
8	T_4,($T_4 - T_3$), ($T_4 - T_5$), ent (T_4)	0.61	0.56
9	T_4,($T_4 - T_3$), ($T_4 - T_5$), ent (T_4), asm (T_4), μ ($T_4 - T_5$), ent ($T_4 - T_5$)	0.67	0.63

Two points are evident from the table. Firstly, that the addition of spatial features significantly improves the skill of the cloud classification, and secondly, that it is possible to define a nighttime algorithm which has similar skill to that available during daytime hours. However, the skill of the cloud-type classification can be further improved by setting a minimum posterior probability for classification. For the classifier represented by model 9 (the last row in Table 1), setting the minimum a posteriori probability to 0.5 yields a contingency table having a Kuipers Performance Index of 0.68 at the cost of only 11.5% of the sample being unclassifiable.

Fig 2 (a) shows the 0.9 μm (channel 2) image from a section of a NOAA11 pass over the Rakaia weather radar domain on 14 December 1993. The pass is from late afternoon local time and shows evidence of a "southerly buster" propagating up the Canterbury Plains east of the Southern Alps. Some cloud shadows (due to the low sun angle) are evident, as is overlying transmissive cirrus in portions of the south-west quadrant of the image. Fig 2 (b) shows the cloud-classification derived from model 4 of Table 1. As noted in the caption, the saturation of each colour indicates the posterior probability of the selected cloud-class, with full saturation indicating a posterior probability greater than 0.90 and grey, a posterior probability of less than 0.40. Data that cannot be classified are shown as dark grey / black - e.g. the cloud - shadow regions fall into this category, as do the coasts. A number of other aspects of the SRTex classifier are evident in Fig 2 (b). There is little evidence of vacillation

between classes. Cloud free areas on both land and sea are clearly identified (with high posterior probabilities) - the former over regions of even quite steep and complex orography in the northern part of the image. Similarly, the area of marine stratocumulus east of the land mass is confidently classified, as is the evident overlying transmissive cirrus. The line of cumulus and embedded cumulus associated with the leading edge of the southerly buster is also clearly identified. The stratocumulus classification of cloud west of the land-mass is less confident, but probably correct given the meteorological situation.

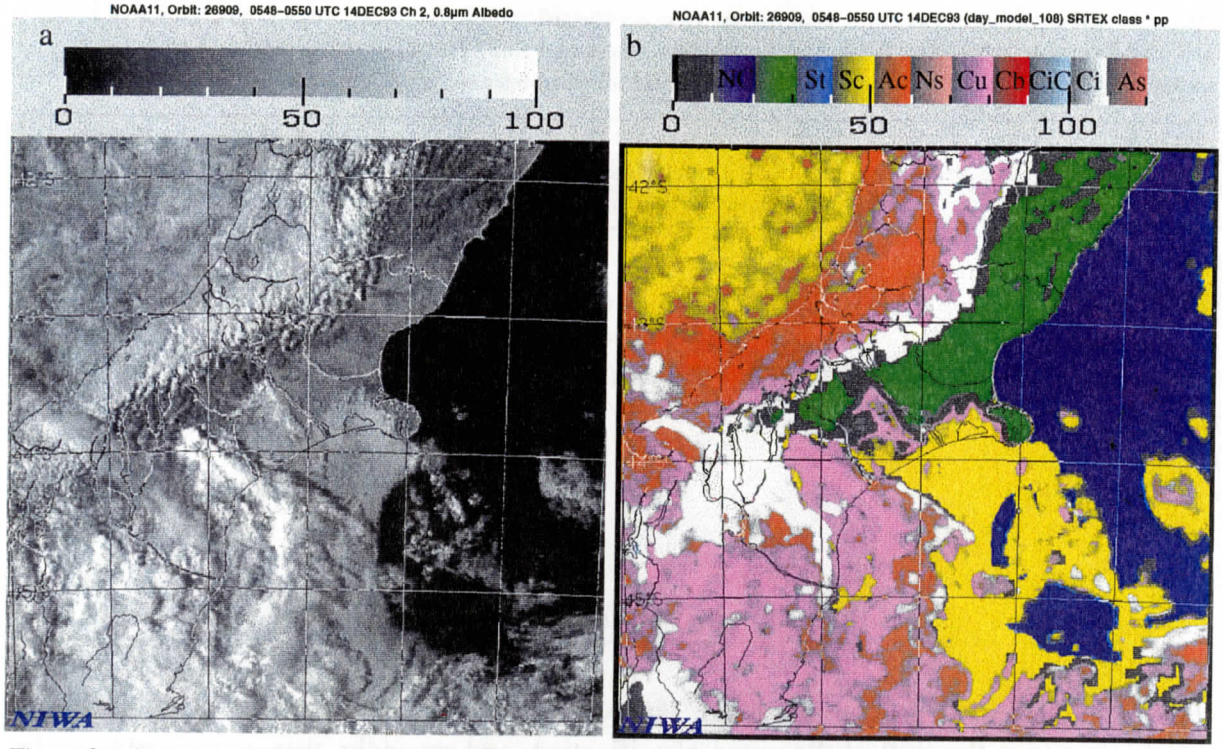

Figure 2: An example SRTex cloud - classification. (a) Channel 2 (0.9 μm) albedo for NOAA 11 pass over Rakaia radar on 14 December 1993. (b) SRTex cloud classification of AVHRR data represented by (a). Each colour indicates the cloud class selected by the Bayesian classifier (see legend above image), while the saturation of the colour is a measure of the posterior probability of the cloud class estimate (saturation falls to grey at a posterior probability of 0.40)

5. RAIN-RATE ESTIMATION

The labelled samples used to derive the cloud-classification discriminant equations include rain-rate data from collocated radar observations, so cloud class specific rain-rate regression equations can be derived using both radiometric and spatial predictors. Clearly some cloud classes do not rain - e.g. stratus, stratocumulus and transmissive cirrus, so the problem of estimating rain-rate from the satellite data is simplified. Rain-rates need only be predicted for those cloud classes known to rain, i.e. classes Ac, Cu, Ns, Cb and CiC. Also, since day time observations can utilise predictors related to cloud albedo, the problem is further separated into day and night sub-problems.

Using linear stepwise regression to identify predictors, and the cube root of the rain-rate as the predictand, rain-rate equations for cloud classes; Ac, Cu, Ns, Cb and CiC were evaluated. All possible spatial and radiative predictors were considered. A summary of the most important daytime predictors and R^2 of the resulting fit are given in Table 2. The night time

equations (not shown) yield significantly poorer fits, having R^2 values in the range 0.2 for class Ns to 0.5 for class Cb).

Table 2: Summary characteristics of the SRTex daytime cloud-type specific rain-rate regression equations where the predictand is third root of the rain-rate. (predictors associated with "max" refer to the tile maximum value of the feature)

Cloud Class	Number of predictors	Most Significant Predictor	R^2
Ac	14	ent (T_4-T_5)	0.60
Cu	11	T_4 max	0.57
Ns	7	R_2 max	0.58
Cb	2	(T_4-T_5) max	0.60
CiC	3	R_1	0.36

Fig. 3 shows scatter plots of measured and (SRTex) modelled rain-rates. While the correlation coefficient (the slope of the line of best fit) is not unity, there is clear evidence (together with the R^2 values) that a reasonable fraction of the rain-rate variance is explained by the SRTex predictions.

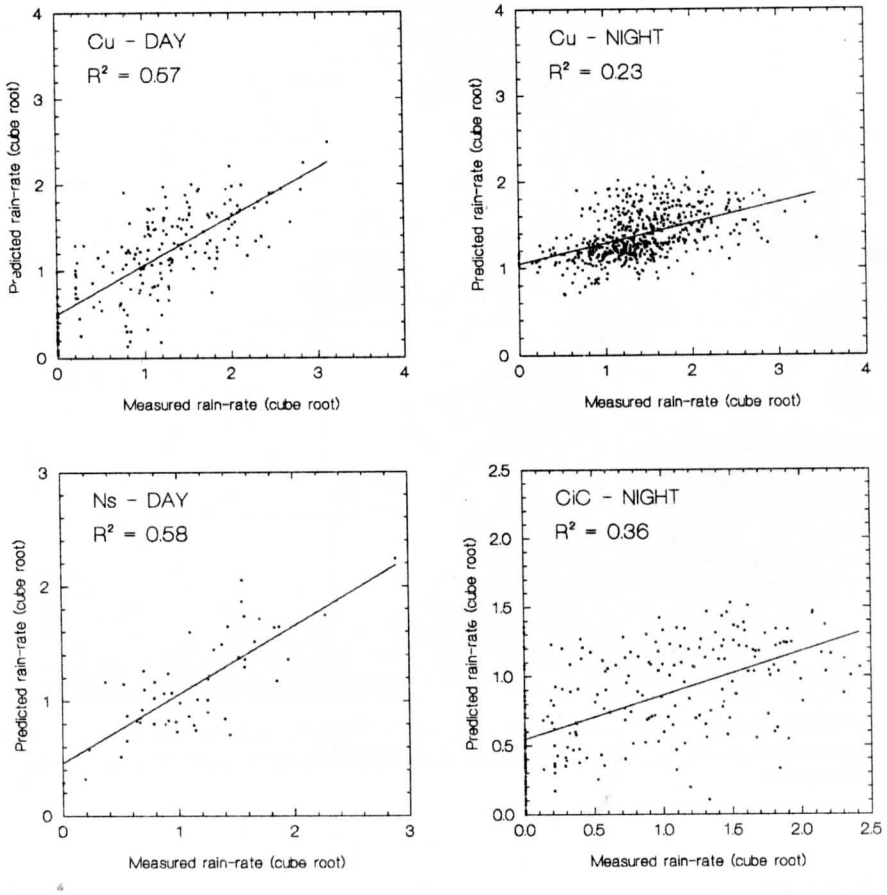

Figure 3: Scatterplots of SRTex predicted and radar measured rain-rates (cube root) for (a) the Cumulus class (daytime), (b) the cumulus class (nighttime), (c) the nimbostratus class (daytime) and (d) the thick cirrus class (nighttime). The line of best fit is also shown.

Fig. 4 shows SRTex rain-rate predictions derived from the cloud-type classification of Fig. 2 (b) and the cloud-class specific rain-rate equations outlined in Table 2. Also included on Fig 4 is a contour analysis of rain visible to the radar (which excludes areas west of the Southern Alps - which rise to over 3000 m). The SRTex analysis appears to have captured most of the rain features evident in the radar data, although toward the edge of the radar domain (in the south-west quadrant - up to 240 km from the radar) the satellite predicted rain-rate intensities are rather low. This could arise from two sources; the low dynamic range of the SRTex predictions and / or problems with the radar vertical profile of reflectivity correction employed in the surface rain-rate estimation procedure.

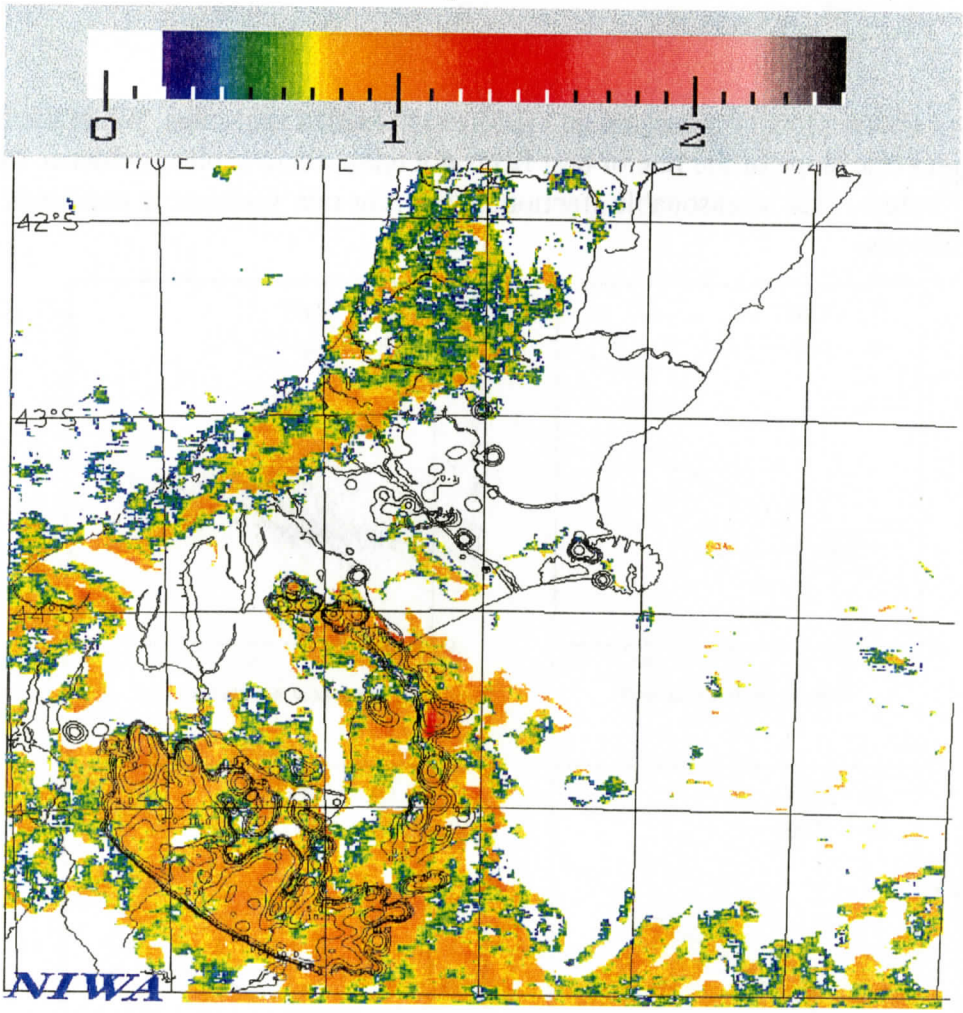

Figure 4: SRTex instantaneous rain-rate predictions for the NOAA11 orbit of Fig. 2 expressed in mm/h overlaid with a contour analysis of the rain-rate as defined by radar (contour intervals are 0.1, 0.5, 1, 2, 5, 10 mm/h)

6. CLOUD DETECTION

Cloud classification using GLD statistics restricts the spatial resolution of the resulting classification, since a tile size smaller than 8 × 8 ifovs is unlikely to yield good estimates of the

spatial characteristics of clouds sampled. However, when only two classes need be identified; clear or cloudy, then the classification can be performed at higher spatial resolution since less use need be made of the spatial information - which is primarily used to discriminate cloud-type. Bayesian discriminant functions were computed from 3 × 3 tiles extracted from the labelled samples of warm cloud (i.e. $T_4 > 0°C$) and cloud-free situations over the areas noted in Fig.1. The skill of the resulting "cloud-mask" classifiers is shown in Table 3.

Table 3: Measures of the skill of day time (Models 1 – 4) and night time (models 5 – 8) cloud-mask classifiers (POD is the Probability of Detection). The prior probabilities were set to 0.5, and all samples were classified. The day time sample size is 590, and the night time sample 1598.

Model No.	Features (where σ refers to the tile standard deviation of the feature)	POD (cloud)	POD (clear)	Kuiper's Performance Index
1	R_2	0.65	0.99	0.63
2	R_2, T_4	0.72	0.99	0.71
3	R_2 , $\sigma(T_4)$	0.94	0.97	0.91
4	R_2, T_4, $(T_4 - T_5)$, $\sigma(R_2)$, $\sigma(T_4)$	0.99	0.98	0.96
5	T_4	0.67	0.84	0.51
6	T_4, $\sigma(T_4)$	0.70	0.97	0.68
7	T_4, $(T_4 - T_5)$, $(T_4 - T_3)$	0.90	0.93	0.83
8	T_4, $(T_4 - T_5)$, $(T_4 - T_3)$, $\sigma(T_4)$	0.94	0.98	0.92

Evidently Bayesian classifiers can be specified which have similar skill for both day and night measurements and have high probabilities of detecting (POD) cloud. The importance of the spatial features is also evident. Additionally, classifier skill can be improved further by limiting the minimum posterior probability for a classification (with the ifov being classified as unknown if it does not reach this threshold). For example, raising the posterior probability threshold to 0.95 for model 8 in Table 3 improves the probability of detecting both cloudy and clear ifovs to 0.99 and the Kuiper's Performance index to 0.97, at the expense of only 10% of samples being unclassifiable.

7. CONCLUSIONS

The results shown here indicate that AVHRR radiometric and spatial features can be used in Bayesian classifiers to determine cloud-type with high skill during both day and night hours. Additionally the skill of different discriminant models can be objectively evaluated. These skill levels might also be expected to be realised in independent data since the labelled training sample spans a very large set of meteorological conditions. Application of a discriminant model to an AVHRR scene further suggests that the cloud classifications are both spatially stable and reasonable.

During daylight hours, rain-rates derived from AVHRR radiometric and local spatial features using cloud class (i.e. Ac, Cu, Ns and Cb) specific prediction equations, are able to explain more than 50% of the variance in coincident radar estimates of the rain-rate. This true for both land and sea samples. During night hours, the reduced spectral information

available reduces the skill of the predictions to about half this value. However, only about 35% of the variance in the rain-rate under thick cirrus can be predicted from the AVHRR data - a not unexpected result given the decoupling between the rain-producing clouds and the measurements. From these results it might be expected that high resolution AVHRR measurements will be able to provide estimates of rain areas and cloud-types within AMSU-A and B ifovs.

Using a similar Bayesian approach, high resolution cloud-masks can be determined through the application of a two state classifier (clear and cloudy) that utilises radiometric and spatial features. The skill of night and day models is similar, and by limiting clear classifications to those ifovs where the posterior probability that it is cloud free is greater than 0.95 yields a POD for cloud of 0.99. This approach is expected to yield very accurate estimates of cloud cover within HIRS ifovs leading to important improvements in the estimation of clear radiances for partly cloud fields of view.

Acknowledgements This research was funded by the New Zealand Foundation of Research Science and Technology.

8. REFERENCES

Grody, N.C., F. Weng and R. Ferraro, 1996: Comparisons between SSM/I, SSMT/2 and radar measurements over the United States. In the *Eighth Conference on Satellite Meteorology and Oceanography,* 28 Jan. – 2 Feb. 1996, Atlanta, GA. Pub. Amer. Meteor. Soc. 243 - 247.

Menzel, W.P., 1993: Trends in global cirrus inferred from three years of HIRS data. In the *Technical Proceedings of The Seventh International TOVS Study Conference,* Igls, Austria, 10 - 16 February, 1993. 319 - 330.

Murphy, A.H., and R.W. Katz: *Probability, statistics and decision-making in the atmospheric sciences.* Westview Press, 545 pp.

Parikh, J., 1977: A comparative study of cloud classification techniques. *Rem. Sens. Env.,* **6**, 67 – 81.

Planet, W.G. (Ed), 1988: Data extraction and calibration of TIROS-N/NOAA Radiometers. *NOAA Tech. Memo. - NESS 107 - Rev 1.*

Rossow, W.B. and R.A. Schiffer, 1991: ISCCP Cloud data products. *Bull. Amer. Meteor. Soc.,* **72**, 2-20.

Stowe L.L., E.P. McClain, R. Carey, P. Pellegrino, G.G. Gutman, P. Davis, C. Long and S. Hart. 1991: Global distribution of cloud cover derived from NOAA/AVHRR operational satellite data. *Adv. Space Res.,* **11**, (3) 51 – 54.

Uddstrom, M.J. and W.R. Gray, 1996: Satellite cloud classification and rain-rate estimation using multispectral radiances and measures of spatial texture. *J. Appl. Meteor.* **35**, 839 - 858

Uddstrom, M.J., W.R. Gray, R. Murphy, N.A. Oien and T. Murray, 1997: A Bayesian cloud mask for sea surface temperature retrieval, Submitted to *J. Atmos. Oceanic Tech.*

Weszka, J.S., C.R. Dyer, and A. Rosenfeld, 1976: A comparative study of texture measures for terrain classification. *IEEE Trans. Syst. Man. Cybern.,* **SMC-6**, 269 – 285.

TECHNICAL PROCEEDINGS OF

THE NINTH INTERNATIONAL TOVS STUDY CONFERENCE

Igls, Austria

20-26 February 1997

Edited by

J R Eyre

Meteorological Office, Bracknell, U.K.

Published by

European Centre for Medium-range Weather Forecasts
Shinfield Park, Reading, RG2 9AX, U.K.

May 1997